FULL PAPER

Effects of magma-generation and migration on the expansion and contraction history of the Moon

Ken'yo U[1*] ⬤, Hiroki Hasumi[2] and Masaki Ogawa[1]

Abstract

Geological and geodetic observations of the Moon from spacecraft revealed that it expanded by a few km for the first several hundred million years and then contracted later. The period when the planet expanded most coincides with that when the mare volcanism of the Moon was active. Given the high initial temperature of the deep mantle inferred from the giant impact and mantle overturn hypotheses of the Moon, the observed early expansion is difficult to account for by thermal expansion only. To understand the observed radial change of the Moon, we numerically calculated the thermal evolution of a one-dimensional spherically symmetric mantle caused by transport of heat, mass, and incompatible heat-producing elements (HPEs) by migration of magma that is generated by internal heating. The mantle is assumed to be enriched in HPEs at its base in the initial condition. The calculated mantle expands for the first several hundred million years by melting of the deep mantle and upward migration of the generated magma to the uppermost mantle; the top of the partially molten region rises to the depth level of around 300 km, which is shallow enough to generate mare basalts of the Moon. The migrating magma, however, extracts HPEs from the deep interior, and the planet then contracts gradually by cooling and solidification of the partially molten mantle. We obtained a thermal history model that is consistent with the observed history of radial change of the Moon when the initial mid-mantle temperature $T_M \approx 1600$ K and the initial ratio of the concentration of HPEs in the crust to that of the mantle $F_{crst}^* \leq 12$. This model suggests that melting of the deep mantle and upward migration of the generated magma strongly affect the thermal history of the Moon. The model we developed here is a good starting point for constructing more realistic models of the thermal history of the Moon where the effects of heat and mass transport by mantle convection are also considered.

Keywords: Moon, Magma migration, Magma generation, Expansion/contraction history

---

"U" is the family name in the author Ken'yo U.

*Correspondence: u-kenyo0822@g.ecc.u-tokyo.ac.jp

[1] Department of Earth Sciences and Astronomy, University of Tokyo at Komaba, Meguro, Tokyo 153-8902, Japan
Full list of author information is available at the end of the article

U *et al. Earth, Planets and Space*   (2022) 74:78

Page 2 of 16

Graphical Abstract

Spherically symmetric model of the mantle evolution that is consistent with the observed radial change of the Moon.
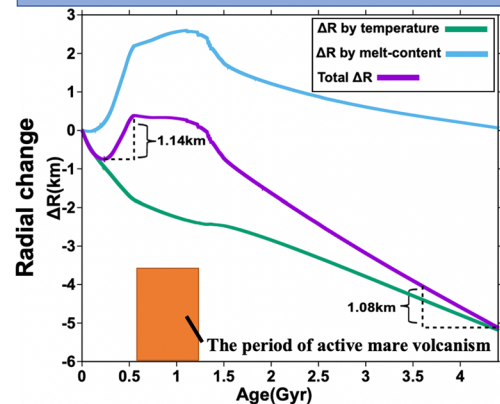
KU, HH, and MO

Observed radial change of the Moon
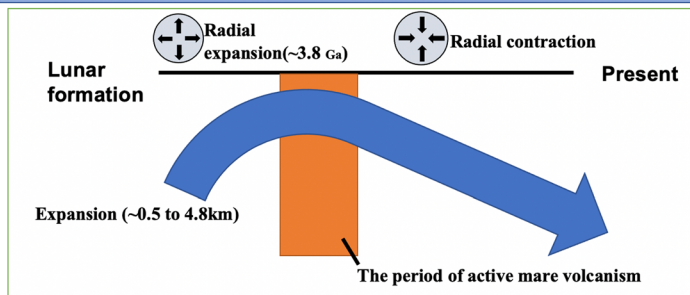
Its expansion is difficult to account for by thermal expansion only.

Considered effects in our model

- The expansion by melting of the mantle
- Magma-generation
- Magma-migration
  - Heat transport
  - Heat-producing elements transport
  - Mass transport   **by migrating magma**

Our model

The calculated melting history accounts for the radial change of the Moon.

The initial state of the favorable models constrains the earliest evolution of the Moon.

Introduction

The thermal history of the Moon has been a long-standing issue in studies of terrestrial planets (e.g., Toksöz et al. 1972; Solomon and Chaiken 1976; Cassen et al. 1979; Kirk and Stevenson 1989; Shearer et al. 2006; de Vries 2012; Evans et al. 2014). Geological and geodetic observations from spacecraft have revealed that the Moon expanded globally in the early stage of its history (Andrews-Hanna et al. 2013; Sawada et al. 2016) and then contracted globally in the later stage (Watters et al. 2010; Matsuyama et al. 2021). The period when its radius reached the maximum coincides with that when the mare volcanism was active: the volcanism was weak before 4 Gyr ago, became active between 3.3 and 3.8 Gyr ago with the peak at ~3.6 Gyr ago, and then mildly continued until 1–2 Gyr ago (e.g., Hiesinger et al. 2003; Whitten and Head 2015). To understand these features of the history of the Moon, we developed a spherically symmetric model of the lunar mantle evolution where magma-generation and migration as well as transport of heat, mass, and incompatible heat-producing elements (HPEs) by migrating magma are considered.

In most of earlier one-dimensional numerical models of the thermal history, the planetary expansion/contraction of the Moon is assumed to occur thermally, and the early expansion is reproduced when the initial temperature in the deep mantle is 1100 K or less (e.g., Solomon and Chaiken 1976): the Moon monotonously contracts throughout its history when the mantle is initially hotter because of secular cooling of the mantle. In a model where the effect of volume change from compositional differentiation is also considered, the early expansion is reproduced even when the initial temperature in the deep mantle is as high as 1200 K (Kirk and Stevenson 1989). However, the initial temperature of 1200 K or less in the deep mantle is still considerably lower than that predicted from the giant impact and mantle overturn hypotheses of the Moon (e.g., Stevenson 1987; Alley and Parmentier 1998; Pritchard and Stevenson 2000; Canup 2004; Rufu et al. 2017; Boukaré et al. 2018; Lock et al. 2018).

The early expansion of the Moon is hard to account for by three-dimensional models of mantle evolution that have been developed in the literature to understand the mare volcanism, too. Some models succeeded in reproducing the peak of mare volcanism at around 3.6 Gyr ago (e.g., Zhong et al. 2000; Stegman et al. 2003; Zhang et al. 2013a, b). Some other models succeeded in reproducing volcanism that continues for billions of years as is observed for the lunar mare volcanism (Konrad and Spohn 1997; Spohn et al. 2001). By considering the blanket effect of the crust, Ziethe et al. (2009) suggest that the

volcanism continues for an even longer period, up to 3.5 billion years. Asymmetric models where the uppermost mantle in the nearside is more enriched in HPEs than that of the farside account for the long-lasting mare volcanism in the Procellarum KREEP Terrane (Wieczorek and Phillips 2000; Laneuville et al. 2013, 2018). The early expansion calculated in these models is, however, too small to account for the observed global expansion of ~0.5–4.9 km until 3.8 Gyr ago (Andrews-Hanna et al. 2013; Laneuville et al. 2013; Zhang et al. 2013a; Sawada et al. 2016), or the early expansion continues too long, 1 billion years or longer (Zhang et al. 2013b).

In these previous models, only the thermal expansion/contraction has been considered, and the planetary expansion by melting has been neglected. The occurrence of dykes and volcanism in the early Moon (e.g., Hiesinger et al. 2003; Andrews-Hanna et al. 2013; Needham and Kring 2017), however, suggests that the effects of volume change from melting are important. Magma migration and transport of heat, mass, and HPEs by migrating magma should also be considered (e.g., Shearer et al. 2006). In this study, we extend the earlier one-dimensional spherically symmetric model of the lunar mantle (e.g., Solomon and Toksöz 1973; Solomon and Chaiken 1976; Kirk and Stevenson 1989) by adding magma-generation and migration and evaluate their effects on the radial change of the planet and volcanism; we start our calculation from a mantle structure predicted from earlier models of the mantle overturn (e.g., Hess and Parmentier 1995; Alley and Parmentier 1998). The model presented here is the first step toward a more comprehensive model of the lunar mantle evolution where mantle convection is also considered.

Model description

To understand the history of the Moon, we numerically calculate a thermal and structural evolution of internally heated one-dimensional spherically symmetric mantle caused by generation and migration of magma, thermal conduction, and internal heating. We take account of transport of heat, mass, and incompatible HPEs by migrating magma, too. The outer radius of the spherical shell r_p is 1740 km, the radius of the Moon, while the inner radius r_c is 383 km, the radius of the lunar core (e.g., Williams et al. 2001; Weber et al. 2011; Yan et al. 2015), and the crust of 43 km in thickness enriched in HPEs is placed along the surface boundary (Wieczorek et al. 2013). The mantle materials are modeled as a mixture of olivine-rich materials A and the ilmenite bearing cumulates (IBC) B (e.g., Ringwood and Kesson 1976); their composition is denoted as $A_{\xi*}B_{1-\xi*}$. The binary system is assumed to constitute a eutectic system with the eutectic composition of $A_{0.1}B_{0.9}$, which corresponds to the

basaltic composition enriched in the IBC component (see Ogawa (2021) for the detail of the thermodynamic formulation). The composition of magma calculated below is almost always eutectic. Magma is generated when the temperature exceeds the solidus temperature. Generated magma migrates upward as a permeable flow through the coexisting matrix driven by the buoyancy of the magma (McKenzie 1984; Kameyama et al. 1996; Ogawa 2018). The temperature is fixed at $T_{sur} = 270$ K on the surface boundary, while the core is modeled as a heat bath of uniform temperature. The thermal diffusivity of the crust is about half that of the mantle and the crust serves as a blanketing layer (Ziethe et al. 2009). Initially, the deep mantle is more enriched in HPEs and IBC-rich component than the mid-mantle as earlier models of mantle differentiation by the magma ocean and the subsequent mantle overturn suggest (e.g., Ringwood and Kesson 1976; Hess and Parmentier 1995). Some earlier studies suggest that a part of IBC-rich cumulates enriched in HPEs remain just beneath the crust after mantle overturn (Yu et al. 2019; Zhao et al. 2019). Instead of explicitly simulating these remains of cumulates, we assume that the crust is uniformly enriched in HPEs.

The basic equations

The continuity equation is:

$$\nabla \cdot \boldsymbol{U} = -\nabla \cdot [\phi^*(\boldsymbol{u} - \boldsymbol{U})]. \tag{1}$$

Here, $\boldsymbol{U}$ is the velocity of the matrix, $\boldsymbol{u}$ that of magma, and ϕ^* the melt-content; $\boldsymbol{U}$ and $\boldsymbol{u}$ have an only radial component because of the assumed spherical symmetry. The relative velocity $\boldsymbol{u} - \boldsymbol{U}$ is proportional to the density difference between magma and the coexisting matrix $\Delta\rho$ as:

$$\boldsymbol{u} - \boldsymbol{U} = -\frac{k_\phi}{\mu\phi^*}\boldsymbol{g}\Delta\rho, \tag{2}$$

where k_ϕ is the permeability that depends on ϕ^* as $k_{\phi 0}(\phi^*/\phi_0^*)^3$ (McKenzie 1984); the ϕ^*-dependence is truncated at its value at $\phi^* = 0.4$. Here, $k_{\phi 0}$ is the reference permeability, the value of which is given in McKenzie (1984) and Miller et al. (2014); ϕ_0^* is the reference melt-content; μ the viscosity of magma; $\boldsymbol{g}$ the gravitational acceleration (the parameter values are given in Table 1). The density difference between solid-phase and melt-phase $\Delta\rho$ depends on the chemical composition of the phases as well as the depth as:

$$\Delta\rho = \rho_0\left\{\beta^*\left(\xi_l^* - \xi_s^*\right) + \frac{\Delta V_l}{V_0}\left[1 + \beta^*\left(1 - \xi_l^*\right)\right]\right\}. \tag{3}$$

Table 1 The meanings of the symbols and their values

Symbol	Meaning	Value
T_{sur}	Surface temperature	270 K
T_0	Melting temperature at the surface	1359 K
r_p	Radius of the surface	1740 km
r_c	Radius of the core–mantle boundary	383 km
r_{crst}	Radius of the Moho	1697 km
ρ_0	Reference density	3300 kg m^{-3}
ρ_{core}	Core density	7500 kg m^{-3}
κ_{mantle}	Thermal diffusivity of the mantle	1.0×10^{-6} m^2 s^{-1}
κ_{edd}	Eddy diffusivity in largely molten regions	50κ at $\phi^* > 0.4$
g	Gravitational acceleration	1.62 m s^{-2}
Δh	Latent heat of melting	657 kJ kg^{-1}
C_p	Specific heat of the mantle	1240 K^{-1} kg^{-1}
C_{pc}	Specific heat of the core	850 K^{-1} kg^{-1}
D_0^*, D_1^*, ς	See Eq. 4	0.11, 0.16, 100 km
$k_{\phi 0}$	Reference permeability	1.0×10^{-14} to 1.0×10^{-13} m^2
ϕ_0^*	Reference melt-content	0.05
μ	Melt viscosity	1 to 20 Pa s
D^*	Partition coefficient of HPEs (solid/melt)	0.01 or 1
α_m	Thermal expansivity in the mantle	3×10^{-5} K^{-1}
α_c	Thermal expansivity in the core	9×10^{-5} K^{-1}

Here, ξ_s^* and ξ_l^* are the content of the end-member A in the solid-phase and the melt-phase, respectively, while ρ_0 the reference density; $\Delta V_l/V_0$ expresses the amount of density reduction by melting and depends on the depth $r_p - r$ as:

$$\Delta V_l/V_0 = D_0^* + D_1^*/\left[1 + \left(r_p - r\right)/\varsigma\right]^2, \qquad (4)$$

where r is the radial coordinate, and the values of D_0^*, D_1^*, ς are chosen so that the solidus temperature calculated from Eq. 4 by the Clausius–Clapeyron relationship (see Eq. 5 below) becomes close to the solidus temperature of mantle materials (Katz et al. 2003; Garcia et al. 2011a, b). We set $\beta^* = 0.135$ based on the density of olivine-rich end-member A ($\rho_{\xi^*=1} = 3300$ kg m^{-3}; Elkins-Tanton et al. 2011), that of the IBC end-member B ($\rho_{\xi^*=0} = 3744$ kg m^{-3}; Snyder et al. 1992; Shearer et al. 2006), and that of the IBC-rich eutectic composition of $A_{0.1}B_{0.9}$ ($\rho_{\xi^*=0.1} = 3700$ kg m^{-3}; Elkins-Tanton et al. 2011; Yu et al. 2019).

The solidus temperature T_{melt} depends on the lithostatic pressure $P = \rho_0 g \left(r_p - r\right)$ as:

$$T_{melt} = T_0(1 + G^*), \qquad (5)$$

where

$$G^* = \frac{1}{\rho_0 \Delta h} \int 0^P \frac{\Delta V_l}{V_0} dP, \qquad (6)$$

T_0 is the solidus temperature at the surface (Katz et al. 2003), and Δh the latent heat of melting.

The energy equation is:

$$\frac{\partial(\rho_0 h)}{\partial t} + \nabla \cdot (\boldsymbol{U}\rho_0 h)$$
$$= -\nabla \cdot \left[\rho_0 h_l \phi^*(\boldsymbol{u} - \boldsymbol{U})\right] - \frac{\Delta V_l}{V_0}\rho_0 \boldsymbol{g}\phi^*\boldsymbol{u} \qquad (7)$$
$$+ \nabla \cdot [k\nabla T + \kappa_{edd}\nabla(\rho_0 h)] + \rho_0 q,$$

where the enthalpy h is written as:

$$h = C_P T + \phi^* \Delta h(1 + G^*), \qquad (8)$$

$h_l = h(\phi^* = 0)$, C_P is the specific heat of mantle materials, T the temperature, $k = \rho_0 C_P \kappa$ the thermal conductivity, κ the thermal diffusivity, and q the internal heating rate. We calculated T and ϕ^* from the value of h calculated from Eq. 7 under the assumption that thermodynamic equilibrium always holds (see again Ogawa (2021) for the detail of the thermodynamic formation of our

U *et al. Earth, Planets and Space* (2022) 74:78

Page 5 of 16

model). We assumed that matrix disintegrates and that a strong turbulent diffusion occurs with the eddy diffusivity of $\kappa_{\text{edd}} = 50\,\kappa$ in largely molten regions with $\phi^* > 0.4$. κ_{edd} is assumed to gradually increase with increasing ϕ^* as ϕ^{*3} to avoid numerical instability. (We confirmed that the radial change we calculated was affected by less than 7% even when κ_{edd} was increased from 50 to 100 κ at $\phi^* > 0.4$). Migration of magma is calculated in the energy equation as a transport of the latent heat of melting by migrating magma (the first term on the right-hand side of Eq. 7). We also assumed that the thermal diffusivity in the crust κ_{crst} is lower than that in the mantle κ_{mantle} to take account of the blanketing effect of the crust and regolith layer (e.g., Ziethe et al. 2009), that is:

$$\kappa = \begin{cases} \kappa_{\text{crst}} & \text{at } r > r_{\text{crst}}, \\ \kappa_{\text{mantle}} & \text{at } r < r_{\text{crst}}. \end{cases} \tag{9}$$

Following the method described in Ziethe et al. (2009), we assumed that $\kappa_{\text{crst}}/\kappa_{\text{mantle}} = 0.48$.

The core is modeled as a heat bath that has a uniform temperature T_c, which changes with time as:

$$C_{pc}\rho_{\text{core}}V\frac{dT_c}{dt} = -Sf, \tag{10}$$

where C_{pc} is the specific heat of the core, ρ_{core} the core density, V the volume of the core, and S the surface area of the core–mantle boundary. The heat flux of the core–mantle boundary f is estimated at the bottom of the mantle as:

$$f = -k\left.\frac{\partial T}{\partial r}\right|_{r=r_c}. \tag{11}$$

The internal heating rate changes with time as:

$$q = q_{\text{tr}}^* q_0 \exp(-\lambda t), \tag{12}$$

where $q_0 = 14.70\,\text{p W kg}^{-1}$ is the average initial heating rate at 4.4 Ga calculated from the total amount of

HPEs in the current Moon, and λ the decay constant (see Table 2). q_{tr}^* changes with time as:

$$\frac{\partial q_{\text{tr}}^*}{\partial t} + \nabla \cdot (q_{\text{tr}}^* \boldsymbol{U}) = -\nabla \cdot \left[\phi^* q_{\text{liq}}^*(\boldsymbol{u} - \boldsymbol{U})\right] + \nabla \cdot (\kappa_{\text{edd}}\nabla q_{\text{tr}}^*), \tag{13}$$

where $q_{\text{liq}}^* = q_{\text{tr}}^*/[\phi^* + D^*(1 - \phi^*)]$, D^* is the partition coefficient of HPEs between melt-phase and solid-phase, and q_{tr}^* is normalized so that $\int_V q_{\text{tr}}^* dV = 1$ holds, where the integration extends over the entire spherical shell. The value of D^* is fixed at 0.01 unless otherwise mentioned (see Table 1 and below).

The bulk composition $\xi_{\text{b}}^* \equiv \phi^*\xi_{\text{l}}^* + (1 - \phi^*)\xi_{\text{s}}^*$ changes with time as:

$$\frac{\partial \xi_{\text{b}}^*}{\partial t} + \nabla \cdot (\xi_{\text{b}}^* \boldsymbol{U}) = -\nabla \cdot \left[\phi^*\xi_{\text{l}}^*(\boldsymbol{u} - \boldsymbol{U})\right] + \nabla \cdot (\kappa_{\text{edd}}\nabla\xi_{\text{b}}^*). \tag{14}$$

In the estimate of the radial expansion of the Moon, we consider the effects of thermal expansion (Solomon and Chaiken 1976) and expansion by melting: the radial change ΔR is given by:

$$\Delta R = \frac{1}{r_p^2}\left[\frac{\alpha_c \Delta T_c}{3}r_c^3 + \int_{r_c}^{r_p}\left(\alpha_m\Delta T + \frac{\Delta V_l}{V_0}\Delta\phi^*\right)r^2 dr\right], \tag{15}$$

where α_c and α_m are the thermal expansivity of the core and that of the mantle, respectively; ΔT_c, ΔT, and $\Delta\phi^*$ are the deviation of the core temperature, temperature in the mantle, and melt-content from the values assumed in the initial condition.

Initial distribution of temperature, HPEs, and bulk composition

Figure 1 shows an example of the initial distributions of enthalpy, temperature, internal heating rate, and composition. This initial condition is motivated by earlier models of the mantle overturn that is expected to have occurred after solidification of the magma ocean (e.g., Snyder et al. 1992; Alley and Parmentier 1998; Elkins-Tanton et al. 2011; Boukaré et al. 2018). Crystal fractionation in magma ocean is expected to have formed a dense layer composed of IBC and urKREEP (materials enriched in K, rare-earth elements, and P) at the top of the mantle. The gravitationally unstable mantle is suggested to have overturned to form a layer enriched in these materials at the base of the mantle (hereinafter, termed the "overturned layer"; e.g., Ringwood and Kesson 1976; Hess and Parmentier 1995; Zhao et al. 2019). The materials in the overturned layer are enriched in HPEs; the overturned materials with the composition of $A_{0.1}B_{0.9}$ are assumed to be 7.5 times more enriched in HPEs than the bulk Moon q_0 (Hess and Parmentier 1995). We estimated the

Table 2 The assumed average content of heat-producing elements (HPEs) in today's bulk silicate Moon

HPEs	heating rate (pW kg^{-1})	Concentration (kg kg^{-1})	Decay constant (Gyr^{-1})
^{238}U	9.46×10^7	21.3×10^{-9}	0.16
^{235}U	5.69×10^8	0.15×10^{-9}	0.98
^{232}Th	2.64×10^7	79.5×10^{-9}	0.05
^{40}K	2.92×10^7	4.39×10^{-9}	0.55

Heating rates and decay constants are after Turcotte and Schubert (2014). We assumed that the lunar bulk Th is the same as a value of the Earth (McDonough and Sun 1995; Tayor and Wieczorek 2014; Laneuville et al. 2018) and then, we estimated the K and U concentrations using the Th/U ratio (Lodders 2003) and K/Th ratio (Tayor and Wieczorek 2014)
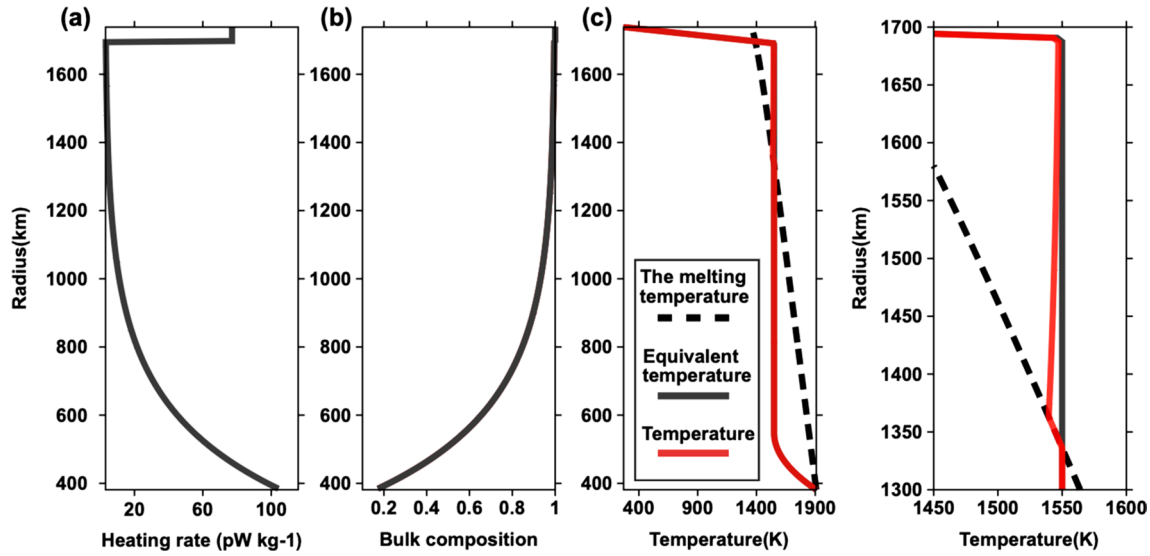
Fig. 1 The initial condition. Illustration of the initial distribution of **a** internal heating rate, **b** bulk composition, and **c** temperature. The assumed parameter values in the figure are: the temperature of the mid-mantle $T_M = 1550$ K; the ratio of the concentration of HPEs in the crust to the mantle $F_{crst}^* = 8$; the thickness of the high-density layer after mantle overturn $L^* = 1/5.5$

distribution of the overturned materials in the mantle after the mantle overturn based on the distributions of internal heat source $q = q_{init}$ calculated in the models of Yu et al. (2019) and Zhao et al. (2019); the initial distribution of q_{tr}^* in Eq. 13 is calculated as q_{init}/q_0. We first approximated the distribution of HPEs they calculated by:

$$q_{init} = q_m + \Delta q \exp\left(-\frac{r-r_c}{l}\right), \tag{16}$$

where $q_m = 2.77$ pW kg^{-1} is the internal heating rate of the olivine-rich materials beneath the layer of IBC and urKREEP before mantle overturn (Yu et al. 2019), l the thickness of the basal layer enriched in the overturned materials, and Δq is calculated from the assumption that the excess internal heating rate in the overturned layer Q_l defined by:

$$Q_l = \int_{r_c}^{r_{crst}} 4\pi r^2 \Delta q \exp\left(-\frac{r-r_c}{l}\right) dr, \tag{17}$$

satisfies,

$$Q_l = \int_{r_c}^{r_p} 4\pi r^2 q_0 dr - \int_{r_{crst}}^{r_p} 4\pi r^2 q_{crst} dr - \int_{r_c}^{r_{crst}} 4\pi r^2 q_m dr. \tag{18}$$

Here, q_{crst} is the average initial heating rate of the crust which is treated as a free parameter (see Fig. 1a). Then, we

calculated the initial distribution of chemical composition ξ_b^* in the mantle from q_{init} as:

$$\xi_b^* = 1 - \frac{\Delta q \exp\left[-(r-r_c)/l\right]}{7.5 q_0}\left(1 - \xi_e^*\right), \tag{19}$$

and $\xi_b^* = 1$ in the crust. Here, $\xi_e^* = 0.1$ is the eutectic composition which is the composition of the magma. On the other hand, the initial distribution of enthalpy h is:

$$h = \min\left(h_{sur}, h_{mantle}\right), \tag{20}$$

where

$$h_{sur} = C_p T_{sur} + E_{sur}\left(1 - \frac{r}{r_p}\right), \tag{21}$$

$$h_{mantle} = \begin{cases} C_p T_M & \text{if } r > r_l, \\ C_p T_M + (T_c - T_M)\left(\frac{r_l - r}{r_l - r_c}\right)^2 & \text{if } r < r_l. \end{cases} \tag{22}$$

(We illustrate the assumed enthalpy distribution in terms of the equivalent temperature $T_{eq} = h/C_p$ in Fig. 1c). Here, the initial temperature in the bulk of the mantle T_M is a free parameter, E_{sur} and r_l are constants arbitrarily chosen to be 6×10^4 J kg^{-1} and 550 km (Hess and Parmentier 1995), respectively, and the initial temperature of the core is $T_c = 1900$ K (e.g., Ziethe et al. 2009; Zhang et al. 2013a, b); we assumed that the core is hotter than the mantle 4.4 Gyr ago (e.g., Alley and Parmentier 1998; Boukaré et al. 2018).

U *et al. Earth, Planets and Space*   (2022) 74:78

Page 7 of 16

Table 3 The variable parameters of the numerical models

Variable parameter	Meaning	Range of value
T_M	Middle mantle temperature	1400–1750 K
M^*	Reference permeability	0–44
F^*_{crst}	The ratio of the concentration of the HPEs in the crust to that in the mantle ($HPEs_{crst}/HPEs_{mantle}$)	4–32
L^*	The thickness of the overturned layer after mantle overturn (see Section "Initial distribution of temperature, HPEs, and bulk composition")	1/5.5–1

The parameters indicated by asterisks are dimensionless

Free parameters

There are four free parameters in our model: the initial temperature in the mid-mantle T_M, the ratio of reference permeability to melt-viscosity $k_{\phi 0}/\mu$ (see Eq. 2), the ratio of the concentration of the HPEs in the crust to the mantle F^*_{crst}, and thickness of the overturned layer l. (The asterisk stands for non-dimensional quantities). Instead of $k_{\phi 0}/\mu$ and l, we will use below their normalized forms $M^* = \frac{k_{\phi 0}\rho_0 g (r_p - r_c)}{\mu \kappa}$ and $L^* = l/(r_p - r_c)$, respectively (Table 3). We varied the normalized permeability M^* in the range estimated from the parameter values of Table 1, F^*_{crst} is estimated from a value adapted in earlier models (Konrad and Spohn 1997; Spohn et al. 2001), and L^* is assumed from a value of the "overturned layer" in earlier models (Fig. 6 of Li et al. 2019; Figs. 6 and 7 of Yu et al. 2019; Fig. 3 of Zhao et al. 2019).

Results

Thermal and structural evolution of the mantle

The reference model

We present the radial change of planet calculated in the reference case in Fig. 2a. The assumed parameter values are $T_M = 1550$ K, $M^* = 28$, $F^*_{crst} = 8$, and $L^* = 1/5.5$. The radius of the planet changes with time by two reasons, thermal expansion and melting (see Eq. 15), as indicated by the green and light blue lines in the figure, respectively. Thermal expansion consistently causes radial contraction of the planet over the calculated 4.4 Gyr history. On the other hand, the history of radial change by melting consists of three stages: in Stage I, the planet rapidly expands until around 0.6 Gyr; in Stage II, the planet slowly expands until around 1.3 Gyr; in Stage III, the planet gradually contracts. In total, the planet expands by 1.23 km because of mantle melting in Stage I but shrinks in Stage III because of thermal contraction and solidification of the mantle; the planet shrinks by 1.08 km for the last 800 million years of the calculated history (the purple line in Fig. 2a).

A closer look at Fig. 2c and e shows more clearly how mantle melting contributes to the calculated radial expansion/contraction history of the planet. The temperature of the deep mantle rapidly increases owing to strong internal heating by the HPEs-enriched overturned layer nearby the core–mantle boundary assumed in the initial condition, and a large amount of magma is generated there. The upward extension of the partially molten region in the deep mantle induced by internal heating and upward migration of the generated magma (Fig. 2c, e) causes the conspicuous radial expansion of Stage I (Fig. 2a). The maximum melt-content of the region is around 0.4 and occurs at the top of the region. The migrating magma concentrates HPEs and the end-member *B* enriched materials to the top of the region (Fig. 2d and f). When the magma enriched in HPEs ascends to the uppermost mantle (radius $r = 1300$–1400 km), however, the effect of conductive cooling from the cold surface boundary overcomes the internal heating by the HPEs in the magma, and the magma solidifies (1.0 Gyr in Fig. 2b); the radial expansion of the planet almost stops accordingly (Stage II in Fig. 2a). According to decay and depletion of the HPEs, the partially molten region then gradually shrinks (Stage III in Fig. 2a).

An interesting feature of the melt-distribution shown in Fig. 2c, e is that two regions with elevated melt-content develop in the mantle after around 1.6 Gyr, one at the radius r around 600 km and the other at r around 1300 km. The shallower region arises because magma migrates upward and causes strong internal heating there by concentrating HPEs. On the other hand, the deeper region arises because upward migrating magma has extracted the compositionally dense end-member *B* from the region by 1.6 Gyr (see Fig. 2f). Because of the depletion in the end-member *B*, the density of matrix becomes almost equal to that of magma that is more enriched in the end-member *B* (see, Appendix 1 for more detail). Owing to the almost neutral buoyancy of magma in the deep mantle, the partially molten region persists there until today (Fig. 2c).

Radial expansion/contraction by magma

To more clearly show how the radial expansion in Stage I and contraction in Stage III of the reference model occur, we calculated three more models, Models 1–3. In Model 1, we switched off magma migration in the reference model by assuming $M^* = 0$ and considered only the effects of thermal diffusion, internal heating, and

U *et al. Earth, Planets and Space*   (2022) 74:78

Page 8 of 16
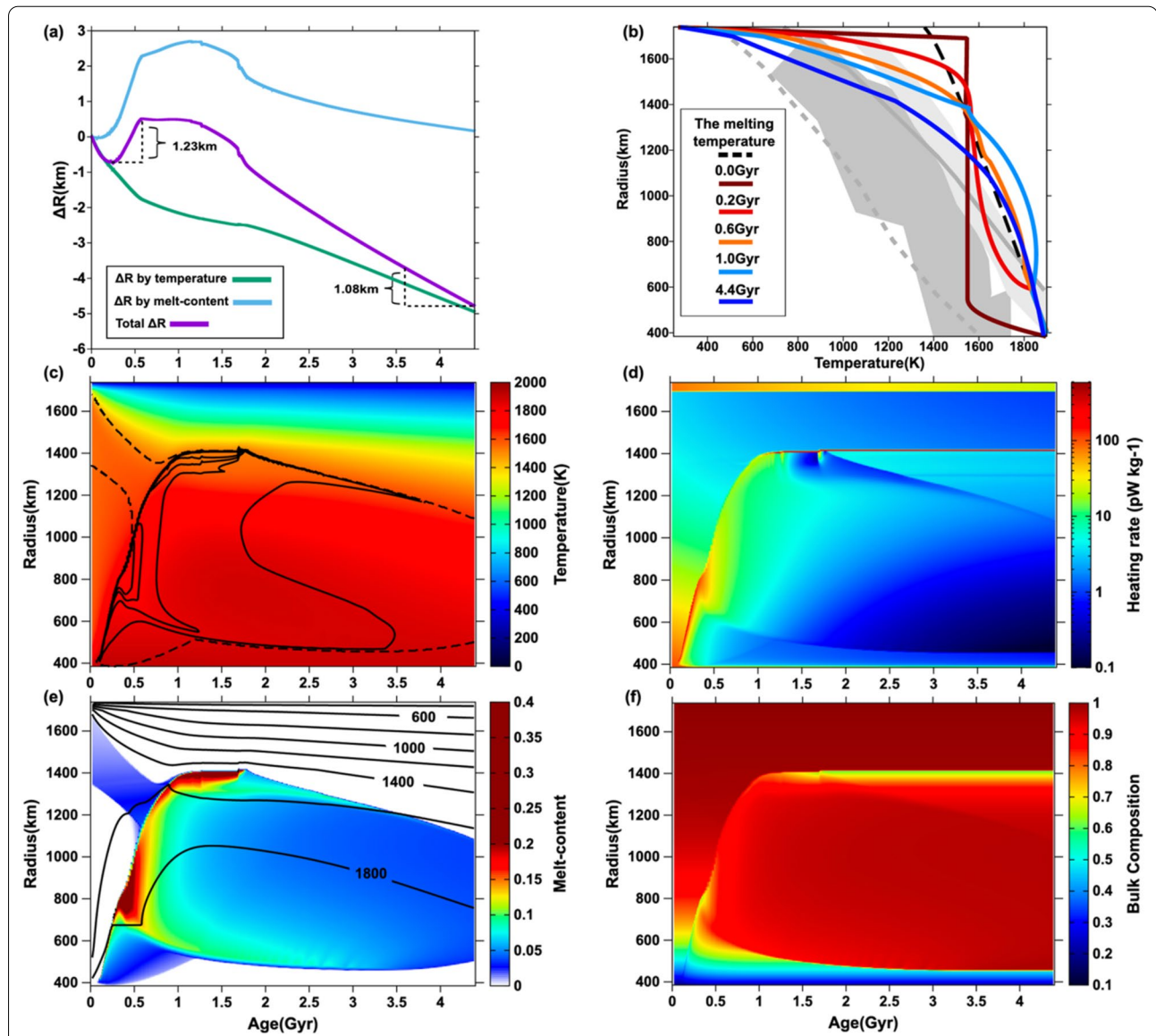
Fig. 2 The reference model. **a** The plot of radius changes against time, **b** temperature profile as a function of time, and the evolution of the distribution of **c** temperature, **d** internal heating rate, **e** melt-content, and **f** bulk composition ξ_b. The assumed parameter values are $T_M = 1550$ K, $M^* = 28$, $F^*_{crst} = 8$, $L^* = 1/5.5$. In **a** the green and light blue lines indicate the contribution of thermal expansion and melting, respectively, to the total radius change (the purple line). In **b** the gray and light-gray areas are the temperature distributions in today's lunar mantle inferred by Khan et al. (2006) and Khan et al. (2014), respectively; the gray lines are those estimated by Karato (2013) under the assumption that the mantle consists of dry olivine (the solid line) and that containing or wet olivine with the H_2O-content of 100 ppm (the dash line). In **c**, the contour lines show the distribution of melt-content with the contour interval of 0.05 starting from 0 (indicated by the dashed line); in **e** the contour lines show the distribution of temperature

melt-generation. In Model 2, we switched on heat transport by magma migration in Model 1 by assigning the default value assumed in the reference model to M^*. We still neglected HPE- and material-transport by assuming $D^* = 1$ in Eq. 13 and fixing ξ^*_b at its initial value; we also assumed $\beta^* = 0$ in Eq. 3 to turn off the effect of compositional density contrast on magma ascent. In Model 3, we added HPE-transport to Model 2 by assigning the default

value to D^* (i.e., $D^* = 0.01$). The difference between the reference model and Model 3 is whether or not the transport of the end-member B by migrating magma (Eq. 14) is taken into account.

In Model 1, the planet first shrinks until around 0.4 Gyr and then expands owing to melting of the deep mantle by internal heating (Fig. 3). A totally molten region develops at the base of the mantle after 0.4 Gyr and becomes

U *et al. Earth, Planets and Space* (2022) 74:78

Page 9 of 16
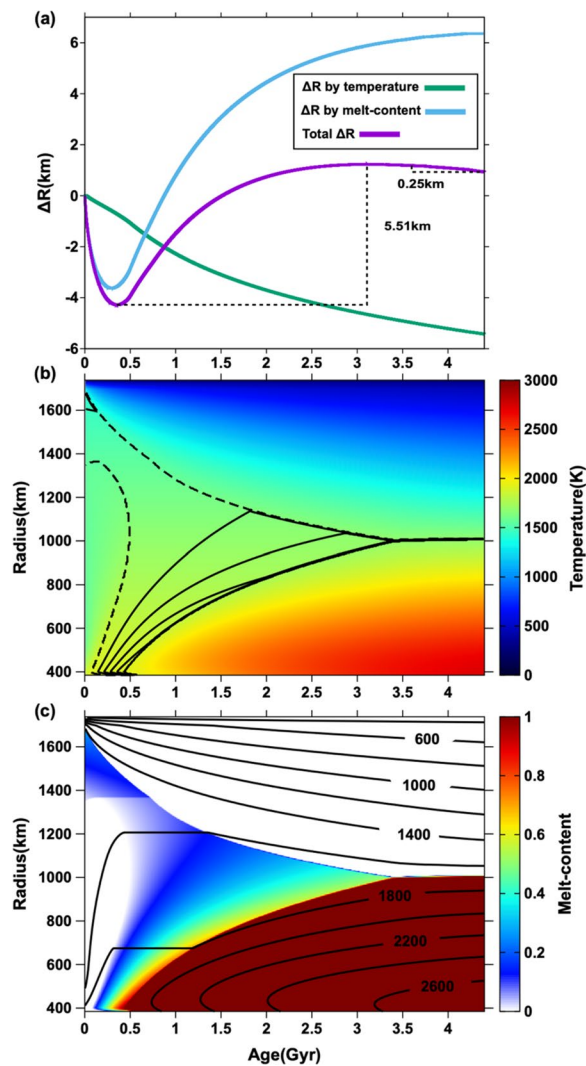
Fig. 3 Model 1. We calculated this model by assuming $M^* = 0$ in the reference model: only the effects of thermal diffusion, internal heating, and melting are considered, and the effects of magma migration are switched off. **a**–**c** Are the same as Fig. 2a, c, and e, respectively. In **b** the contour interval is 0.2 starting from 0 (indicated by the dashed line)
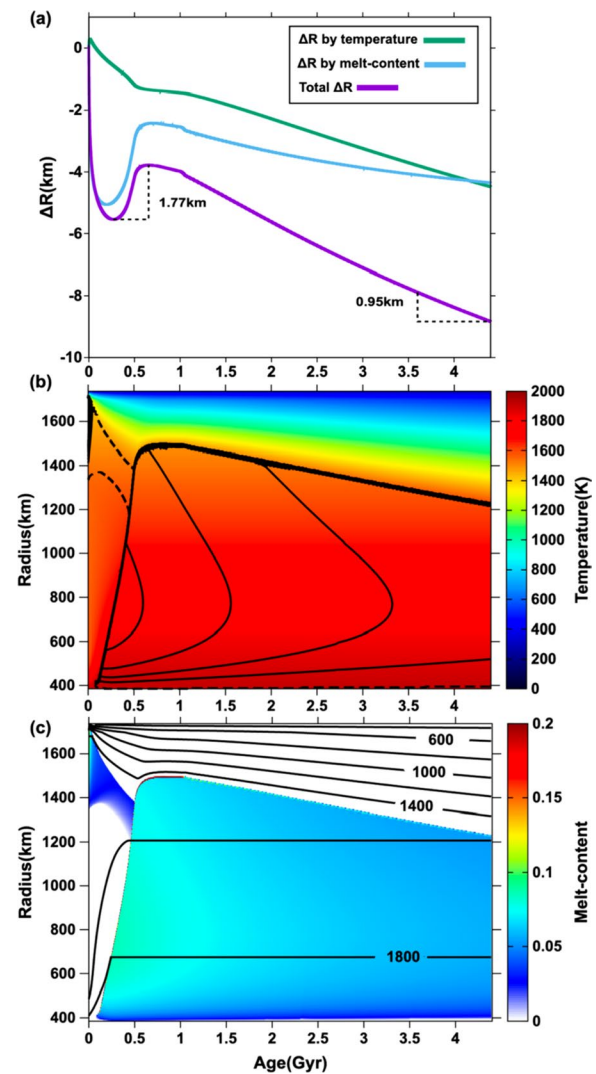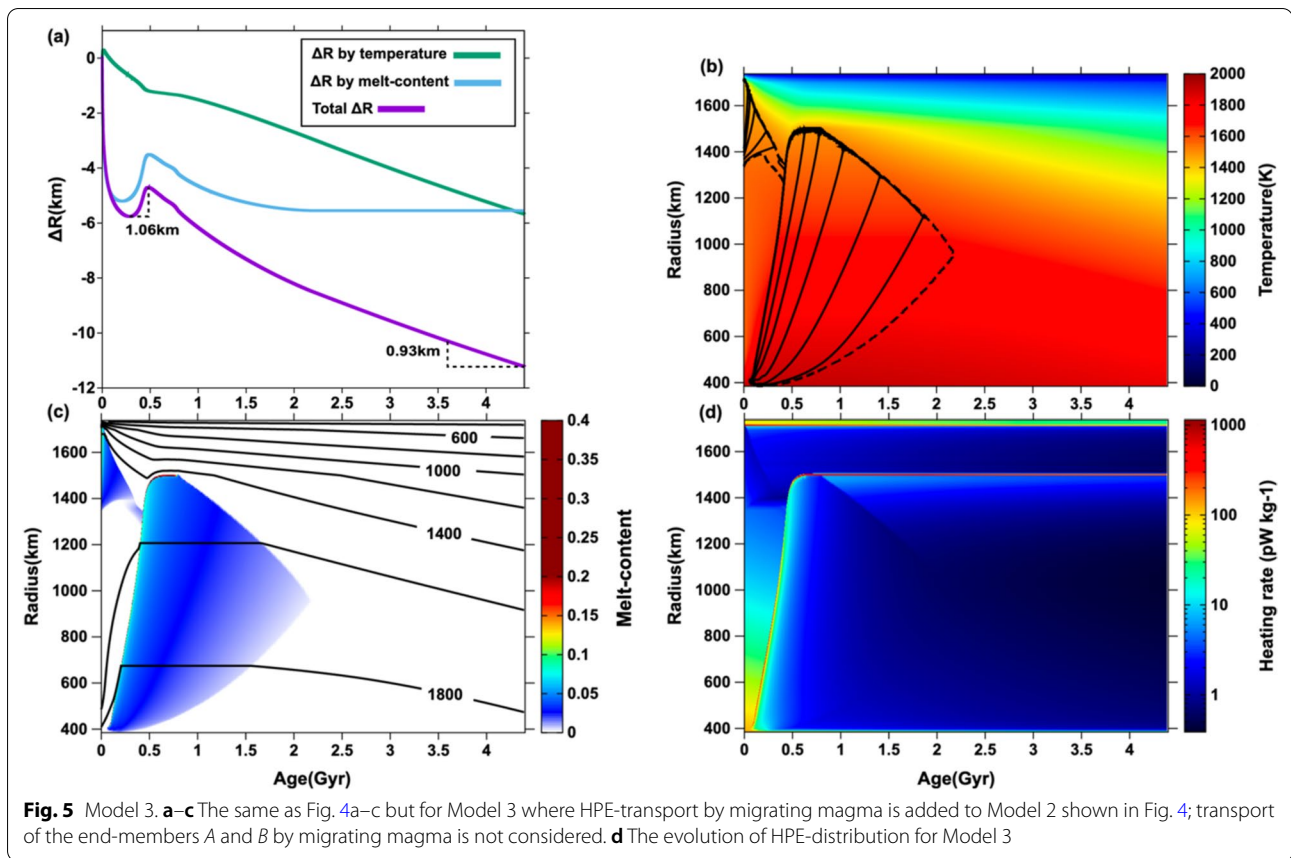

Fig. 4 Model 2. The same as Fig. 3 but for Model 2 where heat transport by migrating magma is added to Model 1 shown in Fig. 3; transport of heat, and the end-members *A* and *B* by migrating magma is not considered. In **b** the contour lines show the distribution of melt with the contour intervals of 0.01 starting from 0 (the dashed lines)

thicker with time because the effect of conductive cooling from the cold surface boundary is negligible at such a great depth; the totally molten region occupies the deeper part of the mantle with radius *r* less than around 1000 km at 4.4 Gyr.

The large-scale melting shown in Model 1 does not occur in Model 2 (Fig. 4) where heat transport by migrating magma is considered. Migrating magma extracts heat from the deep mantle and transports it to the uppermost mantle. The carried heat is further transported to the cold surface boundary by conduction. The melt-content in the deep mantle is less than 0.1, and there is no totally molten region as observed in Model 1. Consequently, the planet radially expands only during the period of ~0.3 to ~0.7 Gyr.

When HPE-transport by migrating magma is also considered (Model 3 in Fig. 5), the partially molten region persists in the mantle only until around 2 Gyr and the entire mantle becomes solid after that. Most of the HPEs in the region migrate upward to the uppermost mantle within the first 0.5 Gyr (Fig. 5d). The magma solidifies quickly at the top of the partially molten region due to the strong conductive cooling from the surface boundary, and the region shrinks

U *et al. Earth, Planets and Space*   (2022) 74:78

Page 10 of 16

Fig. 5 Model 3. **a–c** The same as Fig. 4a–c but for Model 3 where HPE-transport by migrating magma is added to Model 2 shown in Fig. 4; transport of the end-members *A* and *B* by migrating magma is not considered. **d** The evolution of HPE-distribution for Model 3

(Fig. 5b). Note that the early radial expansion by melting observed in Model 3 is 0.17 km, considerably smaller than that observed in the reference model shown in Fig. 2a. The smaller expansion in Model 3 is a consequence of a faster upward migration of magma calculated in Model 3 compared with that calculated in the reference model. Magma velocity is proportional to the density difference between magma and the coexisting matrix (see Eq. 3, Appendix 1). The compositional density difference (the first term on the right-hand side of Eq. 3) is, however, neglected and melt is always substantially less dense than matrix, leading to the faster upward migration of magma in Model 3. The changes of the chemical composition by magma migration also have important influences on the history of the lunar radial expansion/contraction history.

Radial expansion/contraction at various parameter values
We explored how the radial expansion in Stage I and contraction in Stage III depend on the four free parameters, T_M, F_{crst}^*, L^*, and M^* by carrying out an extensive parameter search as shown in Fig. 6.

The initial mid-mantle temperature T_M influences the timing and magnitude of radial expansion in Stage I (Fig. 6a). A higher T_M leads to an earlier occurrence of

expansion with a smaller amplitude and a longer period of contraction (Stage III). This tendency arises because a higher T_M implies a higher melt-content in the initial mantle, which causes earlier expansion of the partially molten region and larger radial contraction due to solidification in the shallow mantle. F_{crst}^* and L^* strongly affect the presence or absence of the expansion. Lower F_{crst}^* and L^* imply more HPEs in the deep mantle, leading to more expansion in Stage I (Fig. 6b, c). The permeability M^* strongly affects the magnitude of expansion/contraction when $M^* \leq 4$ as shown in Fig. 6d because a higher permeability induces quicker drainage of magma from the mantle. (Note that the case at $M^* = 0$ in Fig. 6d is Model 1 in Fig. 3). At $M^* \geq 4$, however, this effect of increasing M^* becomes saturated and the history of planetary expansion/contraction becomes almost independent of M^*.

Discussion
The spherically symmetric mantle calculated in our model radially shrinks for the first ∼300 million years because the magma generated in the shallow mantle by the assumed high initial temperature solidifies. Then, the mantle radially expands by up to 1.49 km ($M^* = 12$
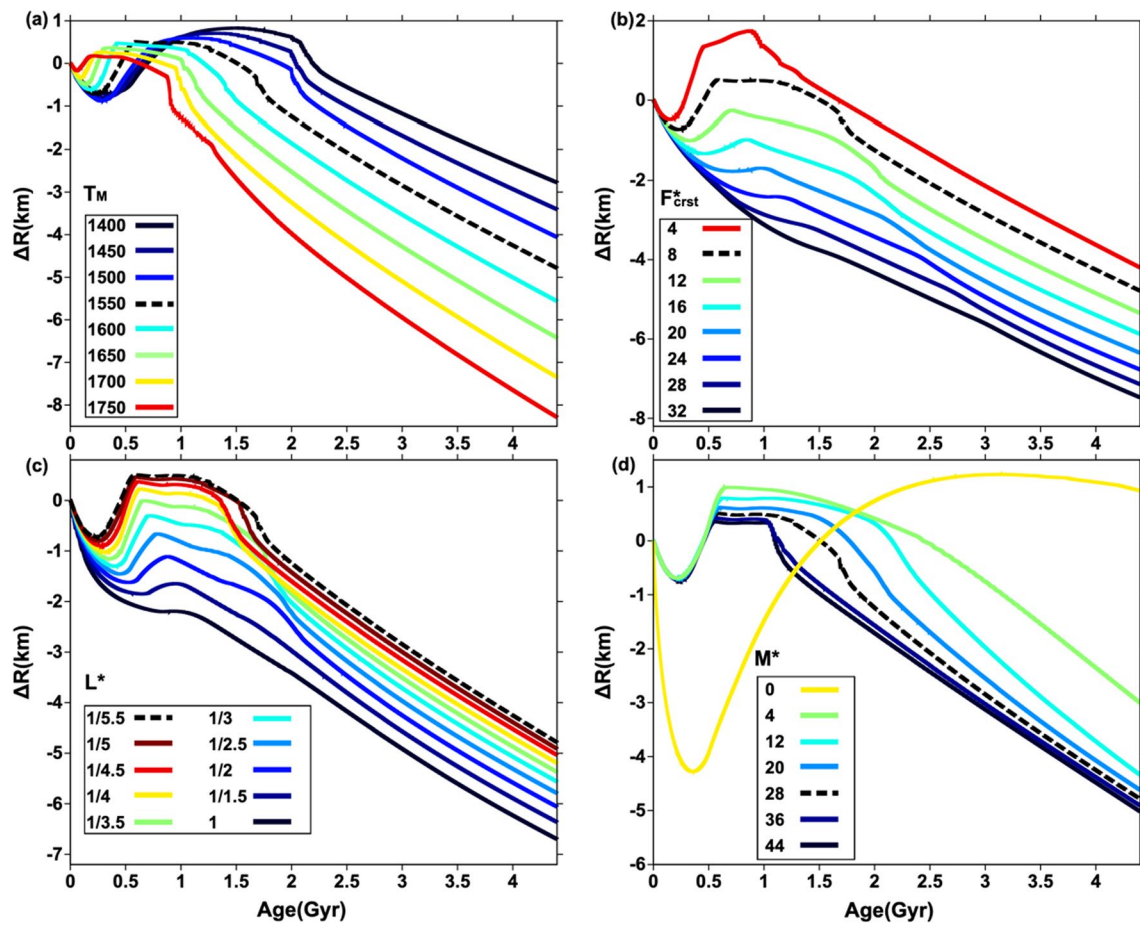
Fig. 6 Radial change at various free parameters. Plots of radial change against time calculated at various values of **a** T_M, **b** F^*_{crst}, **c** L^*, **d** M^*. The dotted lines show the reference model indicated by the purple line in Fig. 2a
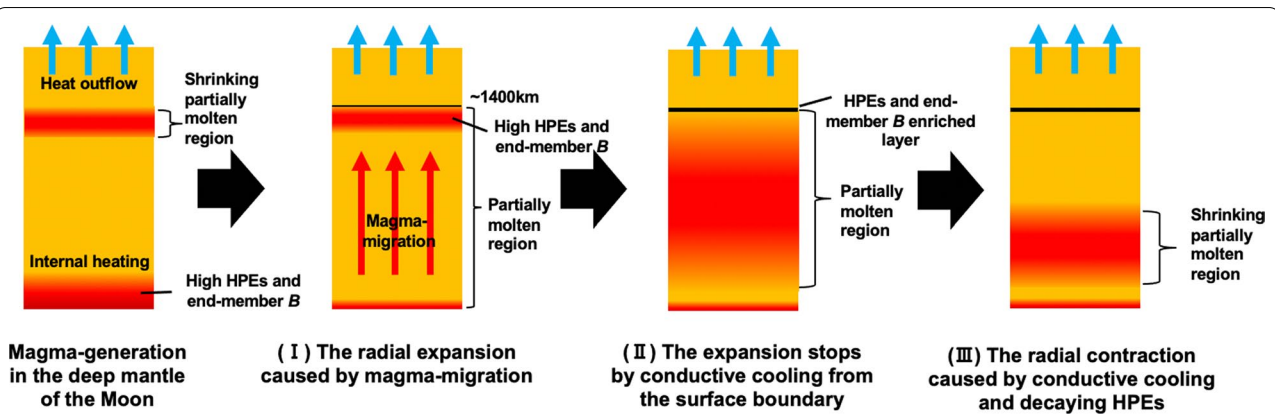
Fig. 7 Illustration of the thermal and structural history of the Moon. For each stage, see Section "The reference model"

U *et al. Earth, Planets and Space*   (2022) 74:78

Page 12 of 16

in Fig. 6d) for several hundred million years as magma is generated in the deep mantle and migrates upward to the uppermost mantle. There, magma is cooled and solidifies by conduction from the surface boundary. Migrating magma extracts HPEs from the deep mantle. After 1–2 Gyr since the start of the calculated history, the mantle radially contracts (∼ 1 km for the last 800 million years) owing to its solidification and cooling that result from the HPE-depletion at depth (see Fig. 7).

Comparison with earlier models

The most important feature of our model is that the mantle radially expands by up to 1.49 km for the first hundred million years in many of the cases where the initial temperature in the mid-mantle T_M is as high as ∼ 1600 K because of the expansion caused by melting. In earlier one-dimensional models where expansion/contraction of the planet occurs only thermally, the initial temperature in the deep mantle must have been less than 600–1200 K at most to account for the early expansion of the Moon (Solomon and Chaiken 1976; Kirk and Stevenson 1989). Otherwise, the earlier researchers found that the calculated mantle monotonously shrinks or only slightly expands at the beginning of its history at most. The same conclusion has been reached in three-dimensional models where heat transport by mantle convection is considered, too. Although the global expansion of the early Moon is as large as 2 km in some earlier models (Zhang et al. 2013a, b), the consumption of latent heat by melting is neglected and the effect of thermal expansion is overestimated in these models. Besides, the early expansion of the model (see H50E100MR2500 of Zhang et al. 2013b, for example) continues for so long as 1 Gyr as is the case for our model that starts with the initial mantle temperature T_M of 1400 K (Fig. 6a); the period of early expansion is substantially longer than that for the Moon. In a model where HPEs are assumed to be enriched in the uppermost mantle of the nearside (Laneuville et al. 2013), the farside mantle shrinks by about 5 km although up to 7 km expansion is observed on the nearside, and this model does not account for the observed global expansion. In our model where planetary expansion by melting is considered, we found a planetary expansion by up to 1.49 km for the first several hundred million years of the calculated history of the mantle (Figs. 2, 6), suggesting that melting of the mantle has played a crucial role in the observed expansion/contraction history of the Moon (Watters et al. 2010; Andrews-Hanna et al. 2013; Sawada et al. 2016; Matsuyama et al. 2021).

Our models also show that a careful modeling of magma-generation and migration is crucial to realistically reproduce the melting history of the lunar mantle. In earlier one-dimensional models where the initial

temperature is more than 1000 K lower than the solidus temperature in the deep mantle (Wood 1972; Solomon and Toksöz 1973; Toksöz and Solomon 1973), a partially molten region is first induced by the high initial temperature in the uppermost mantle and then shifts toward the deep mantle as it is internally heated by HPEs; the mantle becomes totally molten at its base today in some models (see Fig. 6 of Solomon and Toksöz (1973), for example). This melting history is similar to that of Model 1 where the mantle thermally evolves only by thermal diffusion and internal heating (Fig. 3). The melting history, however, substantially depends on magma-generation and transport of heat, HPEs, and materials by migrating magma. When heat transport by migrating magma is added to Model 1, a partially molten region extends upward to the uppermost mantle (Model 2; Fig. 4). When HPE-transport by migrating magma is further considered, the deep mantle becomes depleted in HPEs within around 0.5 Gyr since the beginning of the calculation, and the deep mantle becomes solid within 2 Gyr (Model 3; Fig. 5). In the reference model where changes in the chemical composition by magma segregation are added to Model 3, depletion of matrix in the end-member *B* allows a partially molten region to persist for 4 billion years in the deep mantle (Fig. 2). To account for the melting history of the lunar mantle that exerts control over the history of planetary expansion/contraction and mare volcanism, a careful modeling of magma-generation and migration and the resulting transport of heat, HPEs, and materials by magma is indispensable.

Comparison with the observed features of the Moon

The evolution of partially molten region observed in the reference model that accounts for the radial expansion/contraction history of the Moon (see Fig. 2) meshes with the history of mare volcanism of the Moon. After the initial deepening to the depth of around 400 km until ∼ 0.4 Gyr, the top of a partially molten region in our model becomes shallower and reaches the depth of around 300 km at around 0.8–1.5 Gyr owing to magma migration, and then again becomes deeper with time (Fig. 2c, e). The deepening of the top of partially molten region until around 0.4 Gyr is consistent with the period when mare volcanism on the Moon was not so active (e.g., Hiesinger et al. 2003; Whitten and Head 2015), while its shallow depth at around 0.8–1.5 Gyr accounts for the peak of mare volcanism, which occurred at ∼ 3.6 Gyr ago (e.g., Hiesinger et al. 2000, 2003). The shrinking partially molten region observed after ∼ 1.5 Gyr in our model may correspond to the deepening of the source region of mare volcanism inferred from the variation of Ti concentration in mare basalts (e.g., Hess et al. 1978; Pieters et al. 1980; Taylor 1982; Morota et al. 2011). Although a thermal
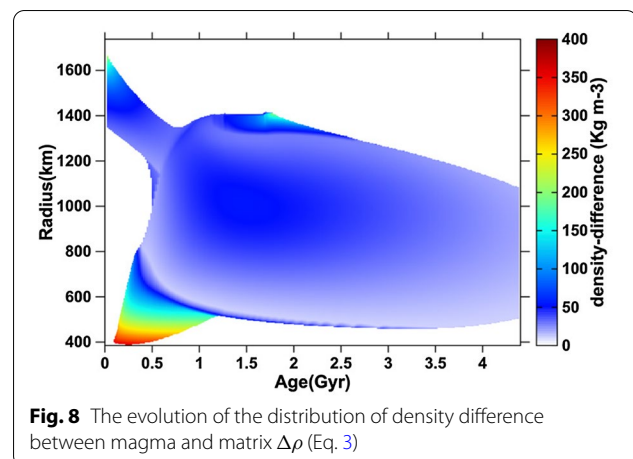
diffusion model where magma generation is not considered also shows the deepening of partially molten region (Wieczorek and Phillips 2000), this earlier model does not account for the weak volcanism of the Moon before about 4 Gyr ago. (Note that this argument is based on an implicit assumption that the activity of the mare volcanism reflects the depth and amount of magma generation in the uppermost mantle. Solomon (1975), however, suggests that the mare volcanism declined since around 3 Ga despite that magma was generated in the mantle because the stress-state in the lithosphere changed and impeded extrusion of the generated magma. Besides, the thickness of the crust and the density contrast between magma and the crust also affect the rate of extrusive magmatism (e.g., Morota et al. 2009; Head and Wilson 2017; Taguchi et al. 2017; Wilson and Head 2017). A more careful modeling of magma migration in the crust and the lithosphere is called for to ultimately resolve the issue of the volcanic history of the Moon).

The profile of horizontally average temperature calculated at 4.4 Gyr in Fig. 2b is consistent with that of today's Moon obtained from analyses of its seismic data and electrical conductivity as a whole (e.g., Karato 2013; Khan et al. 2006, 2014). The presence of a partially molten zone at 4.4 Gyr in our model is also consistent with that in today's mantle of the Moon inferred from its seismic observations (e.g., Latham et al. 1973; Nakamura et al. 1973; Weber et al. 2011). However, the calculated temperature profile is higher than the observed one in the depth range from 700 to 1200 km. Besides, the molten region in our model occurs in the mid-mantle and is ∼ 500 km in thickness with the degree of melting of up to 4% (Fig. 2c, e), while geophysical evidence suggests that the partially molten region occurs at the base of the mantle with its thickness around 150 km and its degree of melting 5–30% (Weber et al. 2011). The differences in the temperature profile and the depth, melt content, and the thickness of partially molten region call for further improvements of the models. In particular, it is important to consider the effects of heat transport by mantle convection.

Possible effects of mantle convection

Constraints on the thermo-chemical state of the lunar mantle just after planetary formation from the thermal history of the Moon have been studied for a long time (e.g., Solomon and Chaiken 1976; Pritchard and Stevenson 2000). Among the models presented in Section "Radial expansion/contraction at various parameter values", those calculated at the initial temperature in the mid-mantle $T_M \approx 1600$ K, the initial crustal fraction of HPEs $F_{crst}^* \leq 12$, and the extent of the enriched layer at the base of the mantle $L^* \leq 1/2$ are consistent with the observed expansion/contraction history of the

Fig. 8 The evolution of the distribution of density difference between magma and matrix $\Delta\rho$ (Eq. 3)
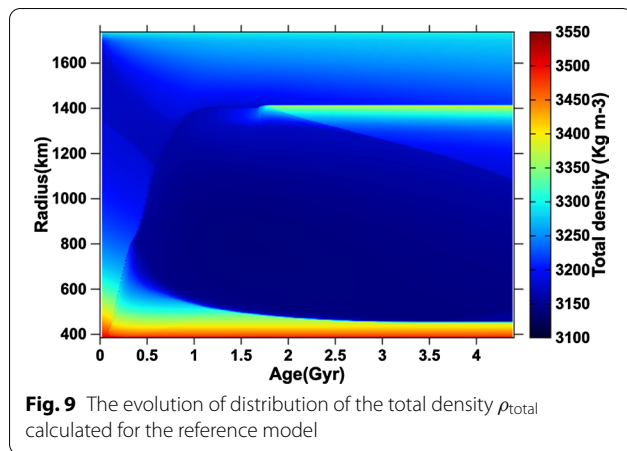
Moon (Watters et al. 2010; Andrews-Hanna et al. 2013; Sawada et al. 2016; Matsuyama et al. 2021). To constrain these quantities more reliably, it is important to add the effects of mantle convection to our model. Many three-dimensional models suggest that evolution of the mantle caused by mantle convection also plays an important role in the thermal and volcanic history of the Moon (e.g., Konrad and Spohn 1997; Spohn et al. 2001; Ziethe et al. 2009; Laneuville et al. 2013, 2018). In particular, the thermal history of the deep mantle is strongly influenced by mantle convection (Stegman et al. 2003; Zhang et al. 2013a, b): migrating magma which is generated in the deep mantle could drive mantle convection of the Moon owing to the buoyancy of the magma; compositional heterogeneity of the mantle caused by magma segregation can also drive mantle convection (see Appendix 1). In the future, numerical models of mantle convection where magma generation and magma migration are considered will be needed for comprehending the thermal and volcanic history of the Moon.

Conclusions

We developed a one-dimensional spherically symmetric numerical model of the thermal history of the lunar mantle, taking magma-generation and migration into account. We found that transport of heat, incompatible heat-producing elements (HPEs), and materials by migrating magma play a crucial role in the thermal history. The planet radially expands by up to 1.49 km during the first around 600 million years in the calculated history as magma is generated in the deep mantle and migrates upward to the uppermost mantle. The migrating magma extracts HPEs from the deep mantle, and the planet then radially contracts due to solidification and cooling of the mantle. The radial expansion/contraction history in our model is consistent with the observed

U et al. Earth, Planets and Space   (2022) 74:78

Page 14 of 16

Fig. 9 The evolution of distribution of the total density ρ_{total} calculated for the reference model

history of the Moon, and the melting history of the mantle in our model accounts for the mare volcanism of the Moon. In future works, it is important to extend our model by taking account of heat and mass transport by mantle convection.

Appendix 1

The density difference in the reference model

We present the density difference between solid-phase and melt-phase $\Delta\rho$ (see Eq. 3) calculated for the reference model in Fig. 8. The density difference is negligibly small at the radius r around 600 km after about 0.5 Gyr, and this small density difference is the reason why magma stays for billions of years there in Fig. 2c and e.

Appendix 2

The density distribution in the reference model

To see how important role mantle convection can play in the thermal history of the Moon, we present in Fig. 9 the total density defined by $\rho_{\text{total}} = (1 - \phi^*)\rho_s + \phi^*\rho_l$ for the reference model, where the density of solid-phase ρ_s and that of melt-phase ρ_l depend on the composition of each-phase and temperature as:

$$\rho_s = \rho_0\left[1 - \alpha(T - T_{\text{sur}}) + \beta^*\left(1 - \xi_s^*\right)\right], \tag{23}$$

and,

$$\rho_l = \rho_0\left\{1 - \alpha(T - T_{\text{sur}}) + \beta^*\left(1 - \xi_l^*\right) - \frac{\Delta V_l}{V_0}\left[1 + \beta^*\left(1 - \xi_l^*\right)\right]\right\}. \tag{24}$$

Figure 9 shows that the layer enriched in the end-member B that develops at the radius of ~ 1400 km after 1.6 Gyr has a negative buoyancy induced by its composition (Fig. 2d and f). The density of this layer ρ_{total} is around 3350 kg m^{-3}, 50 kg m^{-3} higher than the surrounding mantle, and its thickness is around 40 km. The corresponding characteristic time for the Rayleigh–Taylor instability is 0.3–3.3 Gyr when the viscosity of the layer is 10^{20-21} Pa s (see Section "3.1" of Hess and Parmentier 1995). The characteristic time suggests that mantle convection caused by compositional buoyancy can also play important role in the evolution of the lunar mantle.

Abbreviations
HPEs: Heat-producing elements; IBC: Ilmenite-bearing cumulates.

Author contributions
KU and HH developed the numerical code. KU carried out the calculations, analyzed the numerical results, prepared the manuscript. MO supervised the work. KU and MO discussed the numerical results. All authors read and approved the final manuscript.

Authors' information
KU is a graduate student, Department of Earth Sciences and Astronomy, The University of Tokyo at Komaba.

Availability of data and materials
The data and the numerical code of this study are available upon reasonable request to KU (u-kenyo0822@g.ecc.u-tolyo.ac.jp).

Declarations

Ethics approval and consent to participate
Not applicable.

Consent for publication
Not applicable.

Competing interests
The authors declare that they have no competing interests.

Author details
[1]Department of Earth Sciences and Astronomy, University of Tokyo at Komaba, Meguro, Tokyo 153-8902, Japan. [2]Ministry of Internal Affairs and Communications, Chiyoda, Tokyo 100-8926, Japan.

U *et al. Earth, Planets and Space*   (2022) 74:78

Page 15 of 16

References

Alley KM, Parmentier EM (1998) Numerical experiments on thermal convection in a chemically stratified viscous fluid heated from below: implications for a model of lunar evolution. Phys Earth Planet Inter 108(1):15–32. https://doi.org/10.1016/S0031-9201(98)00096-X

Andrews-Hanna JC, Asmar SW, Head JW, Kiefer WS, Konopliv AS, Lemoine FG, Matsuyama I, Mazarico E, McGovern PJ, Melosh HJ, Neumann GA, Nimmo F, Phillips RJ, Smith DE, Solomon SC, Taylor GJ, Wieczorek MA, Williams JG, Zuber MT (2013) Ancient igneous intrusions and early expansion of the Moon revealed by GRAIL gravity gradiometry. Science 339:675–678. https://doi.org/10.1126/science.1231753

Boukaré C-E, Parmentier EM, Parman SW (2018) Timing of mantle overturn during magma ocean solidification. Earth Planet Sci Lett 491(1):216–225. https://doi.org/10.1016/j.epsl.2018.03.037

Canup RM (2004) Simulations of a late lunar-forming impact. Icarus 168(2):433–456. https://doi.org/10.1016/j.icarus.2003.09.028

Cassen R, Reynolds RT, Graziani F, Summers A, McNellis J, Blalock L (1979) Convection and lunar thermal history. Phys Earth Planet Inter 19(2):183–196. https://doi.org/10.1016/0031-9201(79)90082-7

Elkins-Tanton LT, Burgess S, Yin Q-Z (2011) The lunar magma ocean: reconciling the solidification process with lunar petrology and geochronology. Earth Planet Sci Lett 304(3–4):326–336. https://doi.org/10.1016/j.epsl.2011.02.004

Evans AJ, Zuber MT, Weiss BP, Tikoo SM (2014) A wet, heterogeneous lunar interior: lower mantle and core dynamo evolution. J Geophys Res Planets 119:1061–1077. https://doi.org/10.1002/2013JE004494

Garcia RF, Gagnepain-Beyneix J, Chevrot S, Lognonné P (2011a) Very preliminary reference Moon model. Phys Earth Planet Inter 188(1–2):96–113. https://doi.org/10.1016/j.pepi.2011.06.015

Garcia RF, Gagnepain-Beyneix J, Chevrot S, Lognonné P (2011b) Erratum to "very preliminary reference Moon model." Phys Earth Planet Inter 202–203:89–91. https://doi.org/10.1016/j.pepi.2012.03.009

Head JW, Wilson L (2017) Generation, ascent and eruption of magma on the Moon: new insights into source depths, magma supply, intrusions and effusive/explosive eruptions (part 2: predicted emplacement processes and observations). Icarus 283:176–223. https://doi.org/10.1016/j.icarus.2016.05.031

Hess PC, Parmentier EM (1995) A model for the thermal and chemical evolution of the Moon's interior: implications for the onset of mare volcanism. Earth Planet Sci Lett 134(3–4):501–514. https://doi.org/10.1016/0012-821X(95)00138-3

Hess PC, Rutherford MJ, Campbell HW (1978) Ilmenite crystallization in nonmare basalt—genesis of KREEP and high-Ti mare basalt. Proc Lunar Sci Conf 9:705–724

Hiesinger H, Jaumann R, Neukum G, Head JW III (2000) Ages of mare basalts on the lunar nearside. J Geophys Res Planets 105(E12):29239–29275. https://doi.org/10.1029/2000JE001244

Hiesinger H, Head JW III, Wolf U, Jaumann R, Neukum G (2003) Ages and stratigraphy of mare basalts in Oceanus Procellarum, Mare Nubium, Mare Cognitum, and Mare Insularum. J Geophys Res Planets 108(E7):5065. https://doi.org/10.1029/2002JE001985

Kameyama M, Fujimoto H, Ogawa M (1996) A thermo-chemical regime in the upper mantle in the early Earth inferred from a numerical model of magma-migration in a convecting upper mantle. Phys Earth Planet Inter 94(3–4):187–215. https://doi.org/10.1016/0031-9201(95)03102-2

Karato S (2013) Geophysical constraints on the water content of the lunar mantle and its implications for the origin of the Moon. Earth Planet Sci Lett 384(15):144–153. https://doi.org/10.1016/j.epsl.2013.10.001

Katz RF, Spiegelman M, Langmuir CH (2003) A new parameterization of hydrous mantle melting. Geochem Geophys Geosyst 4(9):1073. https://doi.org/10.1029/2002GC000433

Khan A, Maclennan J, Taylor SR, Connolly JAD (2006) Are the Earth and the Moon compositionally alike? Inferences on lunar composition and implications for lunar origin and evolution from geophysical modeling. J Geophys Res. https://doi.org/10.1029/2005JE002608

Khan A, Connolly JAD, Pommier A, Noir J (2014) Geophysical evidence for melt in the deep lunar interior and implications for lunar evolution. J Geophys Res Planets 119(10):2197–2221. https://doi.org/10.1002/2014JE004661

Kirk R, Stevenson D (1989) The competition between thermal contraction and differentiation in the stress history of the Moon. J Geophys Res 94(B9):12133–12144. https://doi.org/10.1029/JB094iB09p12133

Konrad W, Spohn T (1997) Thermal history of the Moon: implications for an early core dynamo and post-accretional magmatism. Adv Space Res 19(10):1511–1521. https://doi.org/10.1016/S0273-1177(97)00364-5

Laneuville M, Wieczorek MA, Breuer D, Tosi N (2013) Asymmetric thermal evolution of the Moon. J Geophys Res Planets 118(7):1435–1452. https://doi.org/10.1002/jgre.20103

Laneuville M, Taylor J, Wieczorek MA (2018) Distribution of radioactive heat sources and thermal history of the Moon. Geophys Res Planets 123(12):3144–3166. https://doi.org/10.1029/2018JE005742

Latham G, Dorman J, Duennebier F, Ewing M, Lammlein D, Nakamura Y (1973) Moonquakes, meteoroids, and the state of the lunar interior. Proc Lunar Sci Conf 4:2515–2527

Li H, Zhang N, Ling Y, Wu B, Dygert NK, Huang J, Parmentier EM (2019) Lunar cumulate mantle overturn: a model constrained by ilmenite rheology. J Geophys Res Planets 124(5):1357–1378. https://doi.org/10.1029/2018JE005905

Lock SJ, Stewart ST, Petaev MI, Leinhardt ZM, Mace MT, Jacobsen SB, Cuk M (2018) The origin of the Moon within a terrestrial synestia. J Geophys Res Planets 123(4):910–951. https://doi.org/10.1002/2017JE005333

Lodders K (2003) Solar system abundances and condensation temperatures of the elements. Astrophys J 591(2):1220–1247

Matsuyama L, Keane JT, Trinh A, Beuthe M, Watters TR (2021) Global tectonic patterns of the Moon. Icarus 358:114202. https://doi.org/10.1016/j.icarus.2020.114202

McDonough WF, Sun S-s (1995) The composition of the Earth. Chem Geol 120(3–4):223–253. https://doi.org/10.1016/0009-2541(94)00140-4

McKenzie D (1984) The generation and compaction of partially molten rock. J Petrol 25(3):713–765. https://doi.org/10.1093/petrology/25.3.713

Miller KJ, Zhu W-l, Montési LGJ, Gaetani GA (2014) Experimental quantification of permeability of partially molten mantle rock. Earth Planet Sci Lett 388(15):273–282. https://doi.org/10.1016/j.epsl.2013.12.003

Morota T, Haruyama J, Honda C, Ohtake M, Yokota Y, Kimura J, Matsunaga T, Ogawa Y, Hirata N, Demura H, Iwasaki A, Miyamoto H, Nakamura R, Takeda H, Ishihara Y, Sasaki S (2009) Mare volcanism in the lunar farside Moscoviense region: implication for lateral variation in magma production of the Moon. Geophys Res Lett 36(21):L21202. https://doi.org/10.1029/2009GL040472

Morota T, Haruyama J, Ohtake M, Matsunaga T, Honda C, Yokota Y, Kimura J, Ogawa Y, Hirata N, Demura H, Iwasaki A, Sugihara T, Saiki K, Nakamura R, Kobayashi S, Ishihara Y, TakedaH HH (2011) Timing and characteristics of the latest mare eruption on the Moon. Earth Planet Sci Lett 302(3–4):255–266. https://doi.org/10.1016/j.epsl.2010.12.028

Nakamura Y, Lammlein D, Latham G, Ewing M, Dorman J, Press F, Toksöz N (1973) New seismic data on the state of the deep lunar interior. Science 181(4094):49–51. https://doi.org/10.1126/science.181.4094.49

Needham DH, Kring DA (2017) Lunar volcanism produced a transient atmosphere around the ancient Moon. Earth Planet Sci Lett 478(15):175–178. https://doi.org/10.1016/j.epsl.2017.09.002

Ogawa M (2018) Magmatic differentiation and convective stirring of the mantle in early planets: the effects of the magmatism-mantle upwelling feedback. Geophys J Int 215(3):2144–2155. https://doi.org/10.1093/gji/ggy413

Ogawa M (2021) The four-stage evolution of martian mantle inferred from numerical simulation of the magmatism-mantle upwelling feedback. J Geophys Res Planets 126:e2021JE006997. https://doi.org/10.1029/2021JE006997

Pieters CM, Head JW, Adams JB, McCord TB, Zisk SH, Whitford-Stark JL (1980) Late high-titanium basalts of the Western Maria: geology of the Flamsteed region of Oceanus Procellarum. J Geophys Res Solid Earth 85(B7):3913–3938. https://doi.org/10.1029/JB085iB07p03913

Pritchard ME, Stevenson DJ (2000) Thermal aspects of a lunar origin by giant impact. In: Canup RM, Righter K (eds) Origin of the Earth and Moon. Univ of Ariz Press, Tucson, pp 179–196. https://doi.org/10.2307/j.ctv1v7zdrp

Ringwood AE, Kesson SE (1976) A dynamic model for mare basalt petrogenesis. Proc Lunar Sci Conf 7:1697–1722

Rufu R, Aharonson O, Perets HB (2017) A multiple-impact origin for the Moon. Nat Geosci 10:89–94. https://doi.org/10.1038/NGEO2866

Sawada N, Morota T, Kato S, Ishihara Y, Hiramatsu Y (2016) Constraints on timing and magnitude of early global expansion of the Moon from topographic features in linear gravity anomaly areas. Geophys Res Lett 43(10):4865–4870. https://doi.org/10.1002/2016GL068966

U *et al. Earth, Planets and Space*   (2022) 74:78

Page 16 of 16

Shearer CK, Hess PC, Wieczorek MA, Pritchard ME, Parmentier EM, Borg LE, Longhi J, Elkins-Tanton LT, Neal CR, Antonenko I, Canup RM, Halliday AN, Grove TL, Hager BH, Lee D-C, Wiechert U (2006) Thermal and magmatic evolution of the Moon. Rev Mineral Geochem 60(1):365–518. https://doi.org/10.2138/rmg.2006.60.4

Snyder GA, Taylor LA, Neal CR (1992) A chemical model for generating the sources of mare basalts: combined equilibrium and fractional crystallization of the lunar magmasphere. Geochim Cosmochim Acta 56(10):3809–3823. https://doi.org/10.1016/0016-7037(92)90172-F

Solomon SC (1975) Mare volcanism and lunar crustal structure. Proc Lunar Sci Conf 6:1021–1042

Solomon SC, Chaiken J (1976) Thermal expansion and thermal stress in the Moon and terrestrial planets: clues to early thermal history. Proc Lunar Sci Conf 7:3229–3243

Solomon SC, Toksöz MN (1973) Internal constitution and evolution of the Moon. Phys Earth Planet Inter 7(1):15–38. https://doi.org/10.1016/0031-9201(73)90037-X

Spohn T, Konrad W, Breuer D, Ziethe R (2001) The longevity of lunar volcanism: implications of thermal evolution calculations with 2D and 3D mantle convection models. Icarus 149:54–65. https://doi.org/10.1006/icar.2000.6514

Stegman DR, Jellinek AM, Zatman SA, Baumgardner JR, Richards MA (2003) An early lunar core dynamo driven by thermochemical mantle convection. Nature 421:143–146

Stevenson DJ (1987) Origin of the Moon—the collision hypothesis. Annu Rev Earth Planet Sci 15:271–315

Taguchi M, Morota T, Kato S (2017) Lateral heterogeneity of lunar volcanic activity according to volumes of mare basalts in the farside basins. J Geophys Res Planets 122:1505–1521. https://doi.org/10.1002/2016JE005246

Taylor SR (1982) Planetary science: a lunar perspective. Lunar and Planetary Institute, Houston

Taylor GJ, Wieczorek MA (2014) Lunar bulk chemical composition: a post-gravity recovery and interior laboratory reassessment. Philos Trans Royal Soc A. https://doi.org/10.1098/rsta.2013.0242

Toksöz MN, Solomon SC (1973) Thermal history and evolution of the Moon. Moon 7:251–278

Toksöz MN, Solomon SC, Minear JW, Johnston DH (1972) Thermal evolution of the Moon. Moon 4:190–213. https://doi.org/10.1126/science.1189590

Turcotte DL, Schubert G (2014) Geodynamics. Cambridge University Press, London. https://doi.org/10.1017/CBO9780511843877

de Vries J (2012) Lunar evolution: a combined numerical modelling and HPT experimental study. USES 14

Watters TR, Robinson MS, Beyer RA, Banks ME, Bell JF, Pritchard ME, Hiesinger H, Bogert CHV, Thomas PC, Turtle EP, Williams NR (2010) Evidence of recent thrust faulting on the Moon revealed by the lunar reconnaissance orbiter camera. Science 329:936–940

Weber RC, Lin P-Y, Garnero EJ, Williams Q, Lognonné P (2011) Seismic detection of the lunar core. Science 331(6015):309–312. https://doi.org/10.1126/science.1199375

Whitten JL, Head JW (2015) Lunar cryptomaria: physical characteristics, distribution, and implications for ancient volcanism. Icarus 247:150–171. https://doi.org/10.1016/j.icarus.2014.09.031

Wieczorek MA, Phillips RJ (2000) The "Procellarum KREEP Terrane": implications for mare volcanism and lunar evolution. J Geophys Res Planets 105(E8):20417–20430. https://doi.org/10.1029/1999JE001092

Wieczorek MA, Neumann GA, Nimmo F, Kiefer WS, Taylor GJ, Melosh HJ, Phillips RJ, Solomon SC, Andrews-Hanna JF, Asmar SW, Konopliv AS, Lemoine FG, Smith DE, Watkins MM, Williams JG, Zuber MT (2013) The crust of the Moon as seen by GRAIL. Science 339(6129):671–675. https://doi.org/10.1126/science.1231530

Williams JG, Boggs DH, Yoder CF, Ratcliff JT, Dickey JO (2001) Lunar rotational dissipation in solid body and molten core. J Geophys Res Planets 106(E11):27933–27968. https://doi.org/10.1029/2000JE001396

Wilson L, Head JW (2017) Generation, ascent and eruption of magma on the Moon: new insights into source depths, magma supply, intrusions and effusive/explosive eruptions (part 1: theory). Icarus 283:146–175. https://doi.org/10.1016/j.icarus.2015.12.039

Wood JA (1972) Thermal history and early magmatism in the Moon. Icarus 16(2):229–240. https://doi.org/10.1016/0019-1035(72)90070-X

Yan J, Xu L, Li F, Matsumoto K, Rodriguez JAP, Miyamoto H, Dohm JM (2015) Lunar core structure investigation: implication of GRAIL gravity field model. Adv Space Res 55(6):1721–1727. https://doi.org/10.1016/j.asr.2014.12.038

Yu S, Tosi N, Schwinger S, Maurice M, Breuer D, Xiao L (2019) Overturn of ilmenite-bearing cumulates in a rheologically weak lunar mantle. J Geophys Res Planets 124(2):418–436. https://doi.org/10.1029/2018JE005739

Zhang N, Parmentier E, Liang Y (2013a) A 3-D numerical study of the thermal evolution of the Moon after cumulate mantle overturn: the importance of rheology and core solidification. J Geophys Res 118:1789–1804. https://doi.org/10.1002/jgre.20121

Zhang N, Parmentier E, Liang Y (2013b) Effects of lunar cumulate mantle overturn and megaregolith on the expansion and contraction history of the Moon. Geophys Res Lett 40:5019–5023. https://doi.org/10.1002/grl.50988

Zhao Y, de Vries J, van den Berg AP, Jacobs MHG, van Westrenen W (2019) The participation of ilmenite-bearing cumulates in lunar mantle overturn. Earth Planet Sci Lett 511(1):1–11. https://doi.org/10.1016/j.epsl.2019.01.022

Zhong S, Parmentier EM, Zuber MT (2000) A dynamic origin for the global asymmetry of lunar mare basalts. Earth Planet Sci Lett 177(3–4):131–140. https://doi.org/10.1016/S0012-821X(00)00041-8

Ziethe R, Seiferlin K, Hiesinger H (2009) Duration and extent of lunar volcanism: COMPARISON of 3D convection models to mare basalt ages. Planet Space Sci 57(7):784–796. https://doi.org/10.1016/j.pss.2009.02.002

Publisher's Note